Thermoelectric energy harvesting from gradients in the earth surface

Journal Article

Author(s):
Sigrist, Lukas; Stricker, Naomi; Bernath, Dominic; Beutel, Jan; Thiele, Lothar

Publication date:
2020-11

Permanent link:
https://doi.org/10.3929/ethz-b-000371857

Originally published in:
IEEE Transactions on Industrial Electronics 67(11), https://doi.org/10.1109/TIE.2019.2952796

Funding acknowledgement:
157048 - Transient Computing Systems (SNF)

Thermoelectric Energy Harvesting from Gradients in the Earth Surface

Lukas Sigrist, Naomi Stricker, Dominic Bernath, Jan Beutel, *Member, IEEE* and Lothar Thiele, *Member, IEEE*

***Abstract*—We introduce an energy harvesting system capable of converting bipolar thermal gradients to electrical energy. An active rectification circuit, electrical impedance matching and commodity thermoelectric generators (TEGs) are used to efficiently extract energy from very small temperature gradients found at the natural ground-to-air boundary. The full harvesting system is modeled in detail from thermal radiation to the electrical load. This end-to-end model enables system dimensioning to meet specific application requirements. A multi-year deployment of the harvesting system supplying a wireless sensor network (WSN) for environment monitoring demonstrates the applicability of this system in a real application. The case study confirms self-sustainable operation of an application with a $550\,\mu\mathrm{W}$ power footprint. With a maximum harvested power of up to $27.2\,\mathrm{mW}$ during the day and $6.3\,\mathrm{mW}$ during the night, a significant improvement in both average and maximum harvested power is demonstrated compared to the state-of-the-art.**

***Index Terms*—Energy harvesting, Energy neutrality, Internet of Things, Rectifiers, System analysis and design, Thermoelectric generator, Wireless sensor networks**

I. Introduction

With significant increases in integration density and energy efficiency the performance of wireless networked sensors has notably improved, enabling more complex applications in the era of Internet of Things. Even with an optimized power footprint the lifetime of a system is constrained by its power requirements and storage capacity. Harvesting energy from the environment provides an unprecedented opportunity to extend application lifetime [1] and reduce maintenance cost, especially for long-term applications typically found in monitoring networks.

This work focuses on harvesting energy using thermoelectric generators (TEGs) which convert heat flux directly into electric energy. TEGs have been used in numerous applications where they exploit the occurrence of process or waste heat. Temperature monitoring of hot pipes by extracting energy from the large temperature gradient they produce was demonstrated in [2]. In [3] a wireless sensor node for building energy management that harvests from wall heaters was developed. Thermal energy harvesting was combined with solar in [4] to increase the power harvested in indoor scenarios. In [5] TEGs were used to power the monitoring blade degradation of band saws. Radioisotope thermoelectric generators rely on radioactive decay of isotopes as heat source and are used as long-term energy supply in space applications [6], [7, Ch. 53-56]. Harvesting from human body heat has been integrated into wristbands [8], clothes [9] and headbands [10] to supply smart watches and vital signs monitoring applications.

Unlike the above applications that exploit waste or process heat, this work's focus is on harvesting energy from naturally occurring gradients found in the ambient at the ground-to-air boundary, i.e. at the boundary of the atmosphere and the earth's surface. Short-term variations in air temperature are generally large compared to temperature changes in the outermost part of the earth surface or objects of the built environment [11]. Radiation is the main driver of gradients found between ground, buildings or other solid objects and the atmosphere. During the day, especially under direct sunlight conditions, a surface exposed to radiation warms up. The radiative energy absorbed at the surface propagates into the material at a rate and with an attenuation depending on the material's thermal conductivity resulting in a thermal gradient. The process reverses at night and is influenced by weather conditions, cloud cover, convection, etc. Therefore, thermal harvesting at the ground-to-air boundary exhibits seasonal patterns with a location dependent magnitude as well as daily patterns that can be exploited. Due to the bi-directional nature of the energy transport, these patterns exhibit different temporal properties than other forms of energy harvesting, e.g. photovoltaics.

Under direct sunlight conditions TEGs cannot compete with photovoltaic cells which have conversion efficiencies that are one order of magnitude higher [12] than those of TEGs [13]. However, by design TEGs are symmetric, bipolar devices, therefore capable of converting both directions of heat flux into electrical energy. Further advantages of TEG based energy harvesting are the utilization of a wide radiation spectrum, the tolerance for partial coverage (e.g. drop shadows, partial snow coverage) and the slow degradation of performance (aging, susceptibility to soiling) [14]. This results in significant energy production at times when other approaches like photovoltaics fail, e.g. at night-time or the transition times between day and night. The nearly continual energy generation of a TEG harvesting based approach widens the design space to systems with only minimal energy storage. Such systems immediately use the harvested energy when it is produced, circumventing the losses incurring with further conversion and storage [15].

Manuscript received May 10, 2019; revised September 16, 2019; accepted October 11, 2019.

This work is evaluated by the Swiss National Science Foundation, and funded in part funded by nano-tera.ch and by grant 157048: Transient Computing Systems and supported by the International Foundation High Altitude Research Stations Jungfraujoch and Gornergrat (HFSJG), 3012 Bern, Switzerland.

Lukas Sigrist, Naomi Stricker, Dominic Bernath, Jan Beutel, and Lothar Thiele are with the Computer Engineering Group, ETH Zurich, Zurich, Switzerland.

Moreover, there are no moving or fragile (glass) parts, no acoustic emissions and the integration with a thermally conductive element and a radiator is simple, resulting in a rugged and highly reliable energy harvesting system.

Therefore, a significant number of previous work has exploited TEGs to extract energy from the temperature gradient occurring in the ambient. In [16] thermal heat flux in soil was analyzed and the authors concluded that thermoelectric harvesting is feasible at the ground-to-air boundary. Subsequently they demonstrated in [17] that thermal harvesters embedded in the upper layers of soil generate an average power of $6\,\mathrm{mW}$ during the summer months using a TEG of undefined type and size. In [18] this scenario was modeled and thereafter experimentally evaluated with a device that had an area of $144\,\mathrm{cm}^2$. They reported an average power of $1.1\,\mathrm{mW}$ before voltage rectification and conversion. In [19], the gradients in the upper soil layers were monitored and through simulations it was concluded that a wireless sensor node can be supplied from only this energy source. Stevens et al. studied the theoretical optimal placement of a harvester at the ground-to-air boundary [20]. In a later experimental study they harvested an average power of $1\,\mathrm{mW}$ with finned thermal guides of $3.8\,\mathrm{cm}$ diameter [21]. By also using a finned heatsink [22] exploited the temperature gradient that occurs in railway tracks due to solar radiation. Meydbray et al. evaluated thermal energy harvesting from the surface-to-ambient gradient and reported an average harvested power of $0.575\,\mathrm{mW}$ for a system with a $131\,\mathrm{cm}^2$ ceramic plate on the ambient side [23]. In [24] the authors performed an experimental study of the heat flux for a ground-to-air harvester with a thermal guide into the soil and a power transistor heat sink on the ambient side. Based on their observations they estimated a peak power of $0.4\,\mathrm{mW}$. A similar study that combined a thermal guide reaching $20\,\mathrm{cm}$ into the ground amd a $17.64\,\mathrm{cm}^2$ sink with a TEG reports a peak power of $50\,\mu\mathrm{W}$ [25]. A convection dominated tunnel wall scenario was modeled and evaluated in [26]. Utilizing the optimized source and load matching, they reported $70\,\mathrm{mJ}$ of harvested electrical energy per day. Datta et al. focused on an asphalt surface to lower soil layer harvesting scenario, and reported up to $16\,\mathrm{mW}$ harvested power around midday utilizing a TEG with an area of $80\,\mathrm{cm}^2$ [27]. Harvesting directly at the pavement surface, the impact of different TEG surface embedding options, surface colors and materials was experimentally evaluated in [28]. Instead of using the ground as a large thermal capacity, it is also possible to use phase changing materials. In [29], [30] the fast changing ambient in an aircraft was used to generate an average power of $22\,\mathrm{mW}$ during an $80\,\mathrm{min}$ flight. Verma et al. harvested at the ambient to water storage boundary [31]. During the summer their systems with a form factor of $101.75\,\mathrm{cm}^2$ generated an average output power of $34.7\,\mathrm{mW}$ in an open environment.

Similar to some of the above mentioned work the thermoelectric harvesting system proposed in this work utilizes a thermal guide to contact lower ground layers. However on the ambient side a black body radiator exploits the large solar radiation during the day and maximizes the emission during night.

Contrary to thermal energy harvesting from process or body heat, where design and operation is governed by one heat flux direction, ambient thermal gradients are primarily driven by radiation that reverses its polarity at least once per day. This results in a bidirectional heat flux through the TEG module and consequently in bipolar output voltages. The small bidirectional temperature gradients of typically only a few Kelvin at the ground-to-air boundary present a veritably challenging harvesting scenario. Under these conditions a TEG generates small bipolar voltages in the $\pm 10\,\mathrm{mV}$ to $\pm 100\,\mathrm{mV}$ range. The voltage levels necessitate efficient low voltage rectification and voltage up-conversion to store the harvested energy in a buffer and/or supply it to an application circuit.

To rectify the voltage before up-conversion the DoupleTip platform [32] uses a harvesting solution that integrates polarity switching into its conversion stage [33]. However the platform has to be optimized at design time for a specific operating point. To enable the use of adaptive unipolar conversion circuits, active rectification is required as traditional diode based rectifications [34, Ch. 1.6] are not feasible for the low TEG voltages. The solution presented in [35] supports cold-starting with a depleted energy storage at the cost of higher quiescent current due to the system's demand for negative voltages. Similar self-powered rectification designs were optimized for efficiency and low quiescent current [36], [37], but require input voltages of several $100\,\mathrm{mV}$.

To maximize the extracted energy, the thermal harvester system has to exploit the largest gradient possible at the ground-to-air boundary, while matching the TEG's thermal resistance for maximum harvesting efficiency. Equivalently, the internal electrical resistance of a TEG has to be matched by the energy extraction circuitry for maximum energy transfer.

Addressing the above mentioned challenges, we make the following contributions in this work:

- We present for the first time an end-to-end model of a thermoelectric harvesting architecture for the ground-to-air boundary. This enables use-case specific optimization for long-term autonomous operation and different power requirements.
- A novel low-power rectification circuit to rectify small bipolar voltages with minimal losses is designed. Experimental evaluation demonstrates its superior performance compared to other semiconductor and mechanical switching solutions.
- We perform in-depth validation of our model. The system components are evaluated individually in a controlled lab environment and the end-to-end model is validated by deploying the system in a concrete wall scenario.
- We provide extensive real-world performance evaluation using a multi-year deployed environment monitoring application. The system used for this study is dimensioned according to our model given the constraints implied by the secenario.

The optimized harvesting system consisting of a thermal guide and a $100\,\mathrm{cm}^2$ radiator is deployed with a fully functional wireless sensor node in a long-term experimental study. The platform harvests up to $27.2\,\mathrm{mW}$ under direct solar exposure, while also providing up to $6.3\,\mathrm{mW}$ during night-time when emitting heat into the ambient. This enables self-

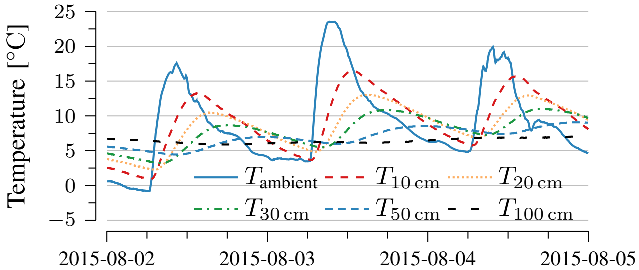

Figure 1. Rock temperature profiles in an alpine rock wall scenario.

sustainable operation of the environment monitoring application with a $550\,\mu\text{W}$ average power footprint that not only senses environmental quantities but also participates in a multi-hop network and communicates the obtained information.

The remainder is organized as follows: an overview of the harvesting scenario and method is given in Section II. The building blocks of the thermal harvesting subsystem are modeled and validated in Section III. Subsequently, Section IV introduces and evaluates the low voltage rectification circuit and completes the end-to-end model with the electrical subsystem. Section V presents a long-term evaluation of the harvesting system with an environment monitoring application, before concluding in Section VI.

II. Thermal Energy Harvesting System

The harvesting system introduced in this work extracts energy from the naturally occurring temperature gradients at the ground-to-air boundary. After specifying the harvesting scenario, an overview of the system and its components is given.

A. Thermal Harvesting Scenario

The surface temperature of rocks and the built environment is governed by radiation and typically follows short-term variable signals [11]. Because the adaption rate decreases with depth in materials with considerably high thermal capacitance, the strong thermal signal present at the surface is attenuated and delayed when propagating through the material. Consequently, a strong bidirectional temperature gradient is observable over the first few centimeters of a surface exposed to radiation that follows a (daily) recurring pattern. This is illustrated with the example of a surface temperature profile recorded in a rock wall environment in Figure 1. The mean annual temperature gradient between the ambient and a depth of $20\,\text{cm}$ in the shown scenario is $0.08\,\text{K}$. Despite the system being in long-term thermal equilibrium, it is possible to harvest energy due to the above mentioned effects. The proposed harvester system adapts its harvesting polarity to the heat flux direction, thus increasing the mean temperature gradient exploitable for harvesting to $3.05\,\text{K}$.

B. Thermal Harvester Architecture

This work presents a thermal energy harvesting platform that exploits the above described temperature gradients using thermoelectric generators (TEGs). The harvesting platform consists of the following components, also illustrated in Figure 2: a TEG (c) is placed between an ambient facing black body radiator (a) that absorbs or emits thermal and solar radiation and a thermal guide (b) connecting the system to the ground at depth. The TEG transduces the resulting heat flux between air and ground into electrical energy. An electrical rectification circuit (d) reverses the polarity of the generator voltage according to the heat flux direction. The voltage converter and battery charge controller (e) converts the low TEG voltages to charge a battery and supply a wireless sensor node application (f).

III. Thermal System Model

The thermal harvesting platform is modeled end-to-end for design exploration and system dimensioning. The model requires meteorological data as input and enables dimensioning a system that supports energy neutral operation of a wireless sensing application. Starting with the thermoelectric generator transducing heat flux into electrical energy, the design and corresponding model of the thermal and radiation components are presented.

A. Thermoelectric Generator Characteristics

Exploiting the Seebeck effect, a thermoelectric generator (TEG) directly converts heat flux resulting from temperature gradients into electrical energy [7]. A TEG consists of p- and n-doped semiconductors with dissimilar thermoelectric properties that are electrically arranged in series and thermally in parallel. Applying a temperature gradient ΔT_{TEG} across the TEG leads to a heat flux through it, resulting in an open-circuit output voltage $V_{\text{TEG,OC}}$ proportional to the gradient ΔT_{TEG}.

$$V_{\text{TEG,OC}} = \alpha_{\text{TEG}} \times \Delta T_{\text{TEG}} \tag{1}$$

The Seebeck coefficient α_{TEG} of a TEG, in units of V/K, is a property of the type and shape of the semiconductor material. For temperature gradients up to several tens of Kelvins, the electrical properties of a TEG can be modeled as a temperature dependent voltage source as in (1) with constant internal resistance R_{TEG} [38]. Consequently, the maximum power is extracted from the TEG when the resistance of the connected load matches the TEG's internal resistance, i.e. $R_{\text{load}} = R_{\text{TEG}}$. The resulting maximum harvested power depends quadratic on the temperature gradient across the TEG:

$$P_{\max} = \frac{(V_{\text{TEG,OC}})^2}{4 \times R_{\text{TEG}}} = \frac{(\alpha_{\text{TEG}})^2}{4 \times R_{\text{TEG}}} \times (\Delta T_{\text{TEG}})^2 \tag{2}$$

Testbed Characterization of TEGs The quadratic behavior of the harvested power for small temperature gradients was verified using a thermal testbed. The testbed consists of two independently controlled Peltier devices and measures the temperature at multiple points in the system as well as the TEG output voltage and current. It allows fully automated replay of dynamic temperature traces that are applied to the device under test for transient system analysis. Overall the testbed provides a consistent environment which is required to characterize and compare commercially available TEGs. The

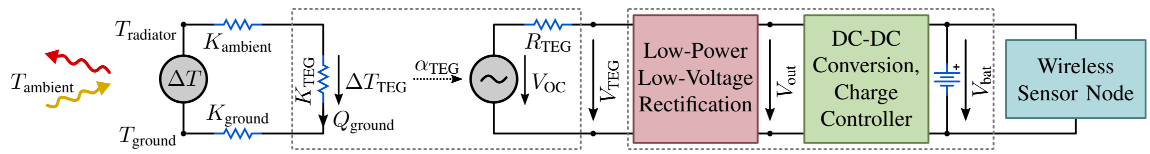

(a) Radiation (b) Thermal Guide (c) Thermoelectric Generator (d) Rectification (e) Voltage Conversion (f) Application

Figure 2. Architecture of the thermal harvesting platform for the ground-to-air boundary: from the radiation regime (a), to the thermal guide (b), the thermoelectric generator (c), and the electrical subsystem (d) and (e) to the application (f).

exploration of considered TEGs provides the foundation for selecting the module best suited for a specific system.

B. Thermal Model of the Harvesting System

The thermal behavior of the harvester is approximated with a lumped parameter model using thermal resistances. It is based on the energy conservation law and assumes steady state conditions and an ideally insulated thermal guide. The thermal resistances of the components are determined by their respective materials and geometries. A two dimensional model was selected to abstract the system and to keep the model complexity and number of parameters manageable. The inclusion of rock and thermal guide capacities, 3-dimensional geometries, and detailed contact properties with and without glue is expected to further improve the model accuracy, but is beyond the scope of this work. The temperatures at the system boundaries, T_{ground} and T_{radiator}, are either measured values or calculated based on the radiation model introduced in the following section. As a result the temperature gradient across the TEG module is calculated as:

$$\Delta T_{\text{TEG}} = \frac{(T_{\text{radiator}} - T_{\text{ground}}) \times K_{\text{TEG}}}{K_{\text{ambient}} + K_{\text{ground}} + K_{\text{TEG}}}, \tag{3}$$

where the thermal resistance on the ambient side is $K_{\text{ambient}} = K_{\text{radiator}} + K_{\text{contact}}$, on the ground side is $K_{\text{ground}} = K_{\text{rock}} + K_{\text{guide}} + K_{\text{transition}} + K_{\text{contact}}$, and K_{TEG} is the thermal resistance of the TEG. Equivalent to the electrical matching, thermal matching, i.e. $K_{\text{TEG}} = K_{\text{ambient}} + K_{\text{ground}}$, maximizes heat flux through the TEG for a given overall temperature gradient [14], resulting in maximum electrical output power (2). The presented thermal model is general to allow using more advanced thermal designs, e.g. heat pipes or a finned design of the thermal guide or a heat sink replacing the black body radiator. Using such an advanced thermal design allows further tuning of the system for a specific scenario and offers the potential for higher harvesting efficiency. In this work the focus is on a simple and highly robust design for deployments in harsh outdoor environments.

Testbed Verification of the Thermal Model The thermal harvester model was experimentally verified using the thermal testbed. For this purpose the thermal system dimensioned for the case study detailed in Section V was used. Forcing of the system boundary temperatures T_{ground} and T_{radiator}, allows evaluation of specific operating points and emulation of real-world traces as shown in Figure 1. As the contact resistance to the rock is not easily integrated and simulated in the testbed, the temperature at the end of the thermal guide is forced directly, therefore corresponding to a $K_{\text{rock}} = 0$ in the model. Comparison of the experimental to the simulation based TEG open-circuit voltage $V_{\text{TEG,OC}}$ in Figure 4 show a close match of modeled and experimental behavior.

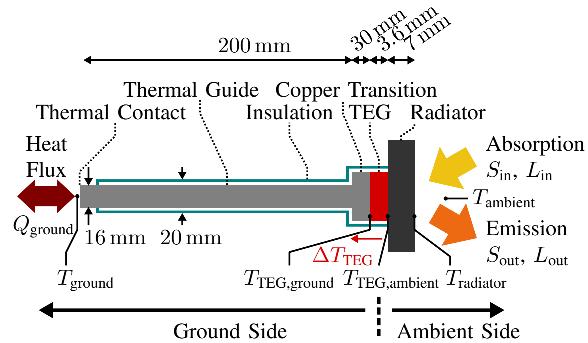

(a) Mechanical structure of the thermal harvester platform (not to scale).

(b) Lumped parameter model for the thermal harvester system.

Figure 3. The components of the lumped parameter model and their corresponding parts in the thermal harvesting platform. The resulting dimensions of the use-case in Section V are shown in the figure.

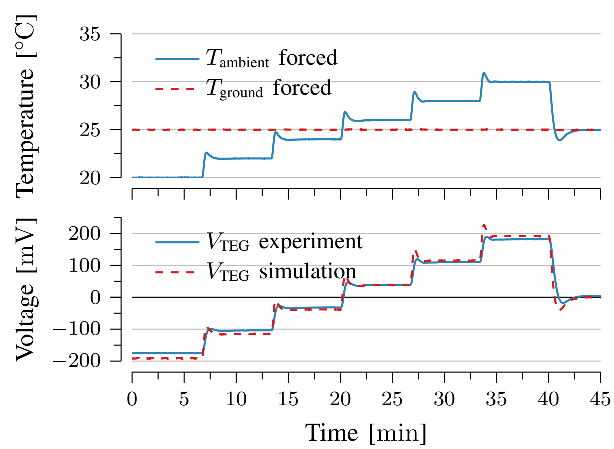

Figure 4. Comparison of testbed experiments and simulations for the thermal model including the characterized TEG. The overshoot of the forced temperature is attributed to the step response of the internal control circuit of the Peltier devices used in the testbed.

C. Radiation Model

The thermal system model is completed by integrating thermal radiation on the ambient side and consequently in-

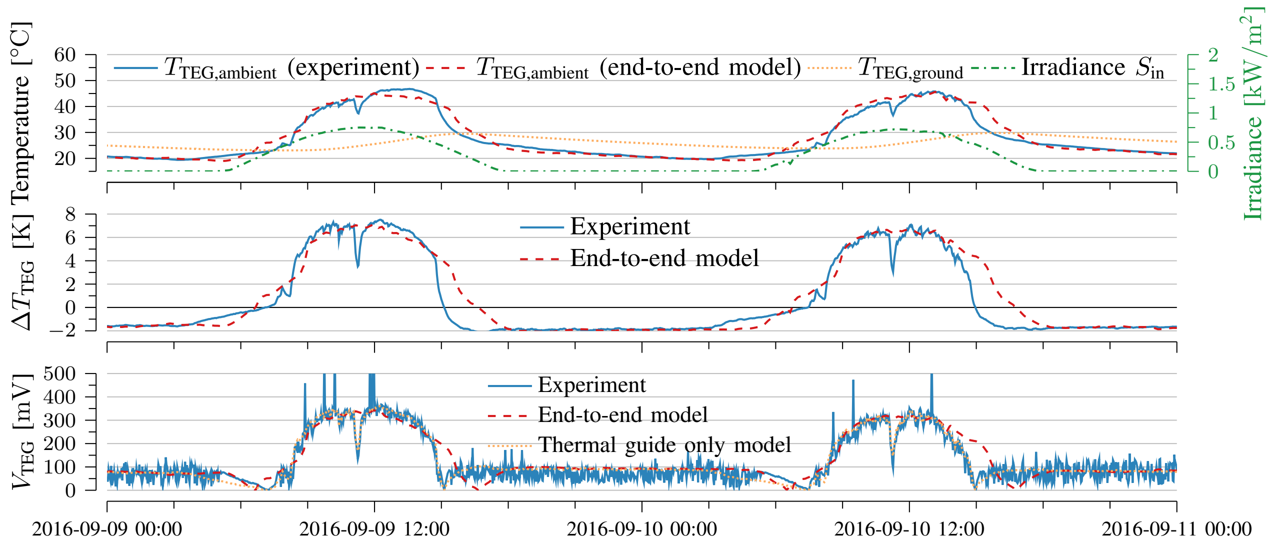

Figure 5. Model verification for two representative days of the urban concrete wall experiment using the end-to-end model from radiation to electrical output and the thermal guide model relying on experimentally observed boundary temperatures.

corporating meteorological data into the model. The radiation model is based on energy conservation which dictates that the incident (short-wave) solar radiation S_{in}, reflected solar radiation S_{out}, absorbed (long-wave) thermal radiation L_{in}, emitted thermal radiation L_{out}, and heat flux through the thermal harvester into the ground Q_{ground} have to be balanced:

$$S_{\text{in}} + S_{\text{out}} + L_{\text{in}} + L_{\text{out}} + Q_{\text{ground}} \equiv 0 \tag{4}$$

The effective incident solar radiation S_{in} and reflected solar radiation S_{out} are derived from the solar radiation corrected by a multiplicative factor $\lambda \leq 1$. This correction factor accounts for the time-varying and deployment specific reduction of the radiation and includes the azimuth, elevation, altitude and visible horizon. For our deployments this factor is determined experimentally. However for high precision models λ needs to be calculated dynamically every few minutes based on celestial data (sun), the true measured horizon, shading, as well as surrounding reflection parameters (albedo) [39]. The thermal radiation L_{in} depends on the air and ground temperature, T_{air} respectively T_{ground}, relative humidity RH, and cloud cover factor φ [40], [41]. The emitted thermal radiation L_{out} is a function of the radiator's temperature T_{radiator} and emissivity $\varepsilon_{\text{radiator}}$. Lastly, Q_{ground} incorporates the thermal model of the harvester which is a function of the harvester's overall thermal resistance K_{tot} and the temperatures T_{ground} and T_{radiator} (Figure 3). Because no closed form solution for T_{radiator} exists, L_{out} is first computed iteratively using a min search algorithm. Then, the radiator temperature is derived using the Stefan-Boltzmann law [42]:

$$T_{\text{radiator}} = \left[\frac{L_{\text{out}}}{A_{\text{radiator}} \times \varepsilon_{\text{radiator}} \times \sigma} \right]^{1/4} - 273.15 \quad [°\text{C}], \tag{5}$$

where $\sigma = 5.67 \times 10^{-8}\,\text{W}\,\text{m}^{-2}\,\text{K}^{-4}$ is the Stefan-Boltzmann constant, A_{radiator} the radiator's surface area and L_{out} the emitted thermal radiation. The radiator temperature T_{radiator} is utilized to compute the resulting temperature gradient ΔT_{TEG} according to (3). Subsequently, the TEG output voltage and its maximum electrical power are derived using (1) and (2).

Radiation Model Verification in Concrete Wall Scenario To validate the full thermal model, the thermal harvesting system, dimensioned for the subsequently examined case study (see Section V), was deployed in an urban concrete wall environment. Two independent harvesters were setup in the southwest (SW) facing artificial retaining wall. The deployed sensor nodes were configured to monitor the temperatures of the wall T_{ground}, the radiator side of the TEG $T_{\text{TEG,ambient}}$ and the thermal guide side of the TEG $T_{\text{TEG,ground}}$. The measured temperature T_{ground} in combination with the incident solar radiation and cloud coverage φ recorded by the close by (900 m) government meteo station enables the simulation of the radiator temperature T_{radiator} and TEG gradient ΔT_{TEG}. The same configuration as in the thermal guide testbed verification is used for the simulation, except that for contact of the thermal guide to the wall using concrete results in $K_{\text{rock}} = 1.25$. The simulation and experiment results are presented in Figure 5: the thermal radiator temperature results are shown on the top and the TEG temperature gradient ΔT_{TEG} in the middle. The graphs demonstrate a good model accuracy for both the radiator temperature T_{radiator} and TEG gradient ΔT_{TEG}. Over the 43 day experiment period their respective mean absolute errors are $5.7\,°\text{C}$ and $0.88\,\text{K}$. The errors can predominantly be attributed to the constrained horizon impacting radiation during morning and evening hours and the drop shadow at approximately 11:00. The bottom plot shows the experimentally observed and modeled optimal voltage at which the TEG is operating, which are discussed in the following sections.

IV. Rectification and Electrical System Model

A novel low power circuit for rectifying the low voltages of thermoelectric generators (TEGs) is introduced and evaluated in detail. Subsequently, the remaining electrical building blocks of voltage conversion and application are discussed to complete the end-to-end model of the harvesting system.

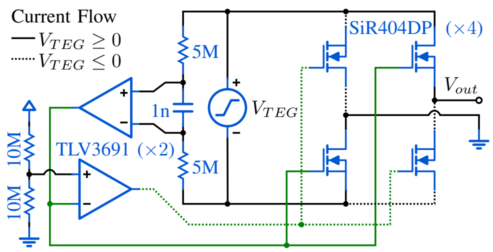

Figure 6. The low-power low-voltage rectification circuit is based on a bridge of four enhancement mode nMOSFETs.

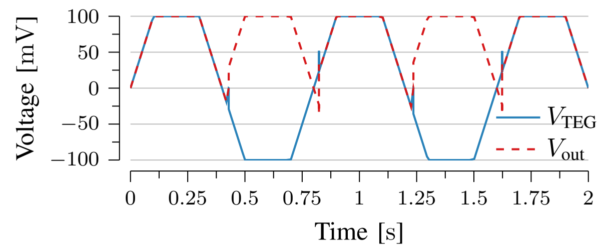

Figure 7. The short-term SPICE simulation confirms the function correctness of the proposed FET-based low-power low-voltage rectification.

A. Low-Power/Low-Voltage Rectification

Because the output voltage of the TEG depends on the heat flux direction (1), the bipolar harvesting scenario results in a bipolar output voltage. This demands for voltage rectification prior to supplying an application circuit. A low resistance rectification solution is key to minimize the losses in the power path. In addition, the low resistance is necessary to enable electrical matching to the TEG's low internal resistance and thus to maximize the harvested power.

Passive rectification circuits based on diodes are not a viable solution due to their forward voltage drop on the order of or higher than the TEG's output voltage. Consequently an actively switched solution with minimal power footprint and power path loss is required. Solutions based on electromechanical switches, commercial solid state SPDT switches and a custom designed MOSFET rectifier bridge are examined and compared with respect to their power path resistance and average power requirement. A control circuit consisting of two TLV3691 nano-power comparators is used for all three approaches, where one comparator observes the polarity of the input voltage and the other generates the inverted control signal.

Despite the considerable switching overhead of electromechanical switches, they provide a competitive solution since the polarity is typically switched only twice a day. The relays as well as the SPDT switches alter which terminal of the TEG is connected to which rectifier output depending on the voltage polarity. For the custom rectification circuit a full active bridge rectifier consisting of four n-type enhancement-mode MOSFETs is built as illustrated in Figure 6. The rectification does not require negative voltage control signals, because the TEG voltage remains at a low level compared to the control circuit supply. This allows keeping the quiescent current draw of the control circuit with $287\,\mathrm{nA}$ at a very low level. As a result the circuit has an ultra low power footprint. Short-term SPICE simulations of the transient behaviour of this solution, shown in Figure 7, confirm the correct operation of the proposed rectifier. Despite the very low switching frequency of typically two times a day, timely switching in the order of seconds is important to adapt to input-voltage inversion for continuous harvesting.

Evaluating Alternative Rectifier Circuits For real-world performance comparison, all three approaches are evalutated experimentally. The results of these experiments are summarized in Table I. The large resistance measured for the SPDT switches leads to considerable power path losses. The proposed MOSFET and the relay solution demonstrate comparable power path resistances. In addition, the MOSFET design has negligible switching power. Although the relays show good performance for the considered metrics, they have significant drawbacks such as mechanical aging, shock sensitivity, unknown properties for very low voltage/current conduction and therefore unknown contact resistance characteristics in long-term operation. Therefore, the proposed MOSFET is considered the best performing solution.

Table I
PERFORMANCE COMPARISON OF DIFFERENT SWITCHING APPROACHES FOR LOW-POWER LOW-VOLTAGE RECTIFICATION.

Method (Type)	$R_{\mathrm{ON,TEG+}}$	$R_{\mathrm{ON,TEG-}}$	avg. P_{q}
FET (SiR404DP)	$0.22\,\Omega$	$0.21\,\Omega$	-
Relay (TXS2-L2-3V)	$0.20\,\Omega$	$0.20\,\Omega$	$23\,\mathrm{nW}$
SPDT (TS3A24159)	$0.71\,\Omega$	$0.67\,\Omega$	$10\,\mathrm{nW}$

B. Electrical Load Matching and Voltage Conversion

The impedance of a harvesting circuit has to match the internal resistance R_{TEG} of a thermoelectric generator to extract power $P_{\max}$ (2) at the maximum power point. The TEG's internal resistance R_{TEG} can, with high accuracy, be assumed constant for low temperature gradients [4]. Therefore the impedance can be matched during the system design phase, or adapted dynamically at runtime using maximum power point tracking (MPPT). In the former case, the input impedance of the circuit is matched to R_{TEG}. For the latter case the input impedance is dynamically adjusted such that the input voltage $V_{\mathrm{in}} = \frac{1}{2} V_{\mathrm{TEG,OC}}$, guaranteeing operation at the maximum power transfer point.

The low temperature gradients of only a few Kelvin, as outlined in Section II-A, lead to input voltages of a few $10\,\mathrm{mV}$ to several $100\,\mathrm{mV}$. This voltage needs to be up-converted in order to charge an energy storage or supply a wireless sensor node application.

Commercially available harvesting management circuits combine these two important aspects and often also incorporate battery charge logic and output voltage regulation. Current solutions for TEG harvesting tend to either be passively controlled coupled-inductor converters or actively controlled single inductor circuits [8]. The former enables harvesting from voltages as low as $20\,\mathrm{mV}$. But their efficiency is limited due to the fixed voltage conversion ratio and internal linear voltage down regulation. The later solution features a dynamic conversion ratio and input impedance matching using MPPT but demands a comparably high minimal input voltage. The bq255xx [43] harvesting management series are based on this principle and implement an ultra-low power control circuit to provide high efficiency at low current draw. Experimental evaluation shows that this particular architecture requires a minimal input voltage for harvesting of at least $60\,\mathrm{mV}$.

For the considered harvesting scenario the bq25570 was selected due to its consistently high efficiency for a wide range of input voltages. The losses incurred by the higher start-up voltage are accepted as a trade-off for the high efficiency for larger input voltages. The bq25570 does not support negative input voltages and hence the TEG output voltages need to be rectified before serving as inputs for the harvesting circuit. The bottom plot in Figure 5 compares the experimentally observed voltage at which power is extracted from the TEG to the voltage at the theoretical maximum power point. The theoretical values of the optimal V_{TEG} are calculated once from the observed temperature gradient ΔT_{TEG} using solely the TEG model (1), and once from the meteorological data using the end-to-end model. The close match of these curves attests optimal load impedance matching and confirms the previously observed high model accuracy from radiation to the electrical energy. The irregularly observed spikes relate to the power point tracking mechanism of the harvester circuit.

C. Wireless Sensor Node Application

An application that performs local sensing and maintains a wireless network to forward recorded data is supplied with the harvested power. It is abstracted as an electrical load that performs duty cycling, a concept widely adopted in low power system design. The energy consumption of the sensor node is modeled by its power consumed during the active and sleep states and the duty-cycle at which the application operates.

V. Thermal Harvesting System for Environment Monitoring Application

For demonstration of the applicability and evaluation of the proposed harvesting architecture the use-case of a wireless sensor node for long-term autonomous environment monitoring in steep rock wall is considered [44]. Specifically, the node monitors itself and senses environmental quantities like temperature profiles at varying depth, movement, thermal and electrical conductivity of rocks, and water pressure inside rocks. In parallel to local sensing the node participates in a multi-hop network and communicates the sensed information and system information like battery level and power consumption through this network. The power footprint for operating such a sensor node is measured to be $550\,\mu\mathrm{W}$.

The end-to-end model detailed Sections III and IV is employed to dimension and implement a harvesting architecture optimized for the considered use-case. Analysis of the specific scenario reveals that the exploitable temperature gradient increases with depth from the ground surface, as well as with the surface area of the radiator. However the system size is strongly restricted by deployment specific boundary conditions such as mechanical mounting and drilling equipment. In the following the details of the dimensioned system are discussed, before extensively assessing its performance in a long-term real-world deployment.

A. System Dimensioning and Integration

Thermoelectric Generator (TEG) A broad range of thermoelectric generators were experimentally characterized. Comparing their performance for low temperature gradients up to $10\,\mathrm{K}$ lead to the selection of a Thermalforce 241-150-29 TEG ($30\,\mathrm{mm} \times 30\,\mathrm{mm}$) with a thermal resistance of $2.27\,\mathrm{K/W}$ and a large Seebeck coefficient of $\alpha_{\mathrm{TEG}} = 111\,\mathrm{mV/K}$.

Thermal Harvester The length of the thermal guide is designed to be $200\,\mathrm{mm}$, the maximum length permitted by the boundary conditions. Two diameters with values up to $25\,\mathrm{mm}$ are utilized. The thermal guide is made of copper due to its excellent thermal conductivity. A copper plate connects the thermal guide with the TEG. The other side of the TEG is in contact with the radiator. A black powder coated aluminum block is used as an approximation of an ideal black body radiator. Furthermore, the radiator is designed to have a large surface area of $100\,\mathrm{mm} \times 100\,\mathrm{mm}$ and a thickness of $30\,\mathrm{mm}$. In addition to absorbing solar radiation and emitting heat, the radiator provides the housing for the thermoelectric generator. The resulting thermal system is of low complexity, mechanically robust, as well as shock proof, thus fulfilling the requirements imposed by the application's environment.

Electrical Subsystem The custom rectification and bq25570 harvesting circuit are integrated into the wireless sensor node. The extracted power is stored in a Saft MP174565 lithium-ion battery. These cells can be charged down to $-30\,^{\circ}\mathrm{C}$ as is necessary for our use-case and allow ample storage to bridge extended periods of energy scarcity.

Application Model and Integration The considered application is modeled as an electrical load with an average power footprint of $550\,\mu\mathrm{W}$. The application is integrated to be solely powered from the harvested thermal energy. The sensor node is configured to monitor the performance of the harvesting platform. The results of these in-situ measurements are presented in the following.

An exploded view of the system designed for the rock wall use-case is shown in Figure 8.

B. Real-World Harvesting Performance

The final system was installed for long-term testing in a field site for high-alpine environmental research at $3\,500\,\mathrm{m\,a.s.l.}$ [11]. Two systems were deployed on a steep southeast (SE) facing and one on a near-vertical northwest (NW) facing rock wall. The system on the NW facing wall, position 31, and one on the SE facing wall, position 29, both had a thermal guide diameter of $16\,\mathrm{mm}$, equal to the one in the urban concrete wall experiment. The second system in the SE facing location, position 28, had a larger diameter of $25\,\mathrm{mm}$. Figure 8 illustrates the deployment of the SE facing position 29.

Overview For each position between 6 and 21 months of data were captured. The average harvested power was $1.21\,\mathrm{mW}$,

Figure 8. Left: exploded view of the system components of the harvesting system consisting of the thermal harvester, TEG, rectification circuitry, and the wireless sensor node (WSN). Right: the system deployed in the rock wall for the long-term case study (photograph of the SE position 29).

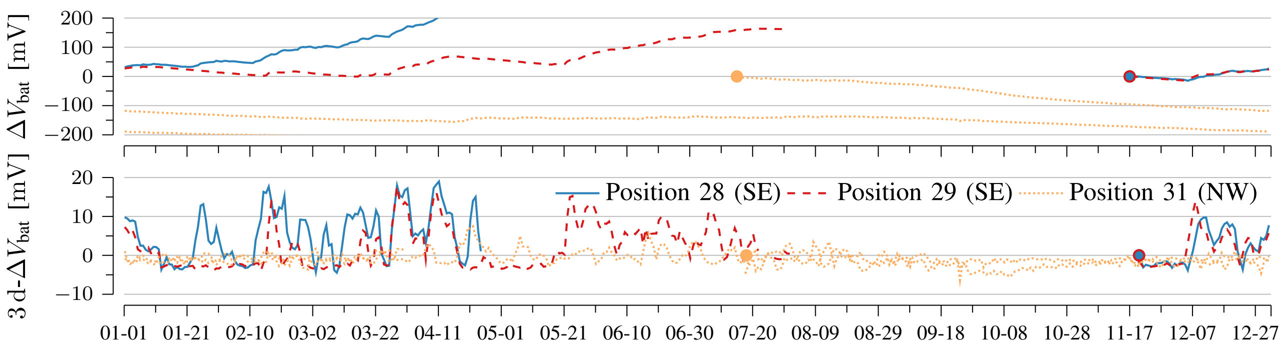

Figure 9. Long- and short-term (3 day differences) battery voltage evolution showing steady charging at south locations.

$1.09\,\mathrm{mW}$, and $0.76\,\mathrm{mW}$ for positions 28, 29, and 31, respectively. The top of Figure 9 shows the evolution of the battery voltage relative to the marked starting point. The lower part depicts the difference of the battery voltage over 3 days to amplify and visualize the momentary dynamics throughout the year. The curves are wrapped around at the end of the year. Periods with steadily decreasing ΔV_{bat} are longer bad-weather periods typically coinciding with a local increase in snow cover. Differences in snow cover result in position 28 starting to generate energy at the beginning of the year before position 29 does despite their proximity. The battery voltage for all posit ions increases during the summer months because of the longer periods of direct incident solar radiation. This effect is more pronounced on the SE than the NW facing deployments. Nevertheless, the NW facing node sustains energy neutral operation during the summer. The harvested energy however is not sufficient to compensate for the harvesting deficit during the winter.

Detail Excerpt The 10 day excerpt from spring 2017 in Figure 10 shows the temperature gradient ΔT_{TEG} across the generator and the total harvested power P_{harv}. Initially, snow cover insulates all three positions resulting in an almost zero ΔT_{TEG}. As the snow cover decreases position 28 starts harvesting more energy on March 19. Position 29 follows the next day. The variability during March 21 indicates variable weather with intermittent cloud cover. During the following four days the nodes are not exposed to direct incident solar radiation because of constant cloud cover. Nonetheless ΔT_{TEG} continues to follow a daily pattern. On March 26, a perfectly sunny day, the SE facing positions 28 and 29 generated a peak power of $25.4\,\mathrm{mW}$ and $26.5\,\mathrm{mW}$, respectively. Because the solar elevation angle increases in springtime, position 31 starts receiving direct sunlight in the late afternoon which the temperature trace reflects. It must be noted that during the time window of the detail excerpt, the harvesting circuit of position 31 malfunctioned resulting in significantly reduced harvested power. However, the temperature measurements show correct values, allowing to draw the above conclusions.

Operation Mode Analysis Lastly, the distribution of the temperature gradients and the generated energy on the SE and NW facing deployments is analyzed. The histograms show the duration the harvester was operating at a given TEG temperature gradient ΔT_{TEG} and the total energy generated during these periods, Figure 11 for position 29 and Figure 12 for position 31. As expected, both systems are in a thermal equilibrium with a mean ΔT_{TEG} close to zero. However, the harvesting relevant mean absolute gradients are $1.59\,\mathrm{K}$ and $0.96\,\mathrm{K}$ for positions 29 and 31. The difference between both positions is mainly attributed to the frequency with which high ΔT_{TEG}, resulting from direct incident solar radiation, occur. The SE facing node harvests most of its energy during periods of high temperature gradients whereas the NW facing node is exposed to high ΔT_{TEG} much less often and therefore harvests most of its energy at lower temperature gradients. We distinguish two operation modes: *net absorption* if the overall heat flux is from the ambient towards the ground, and *net emission* when heat from the ground is emitted into the ambient. The NW facing node operates $43.3\,\%$ of the time

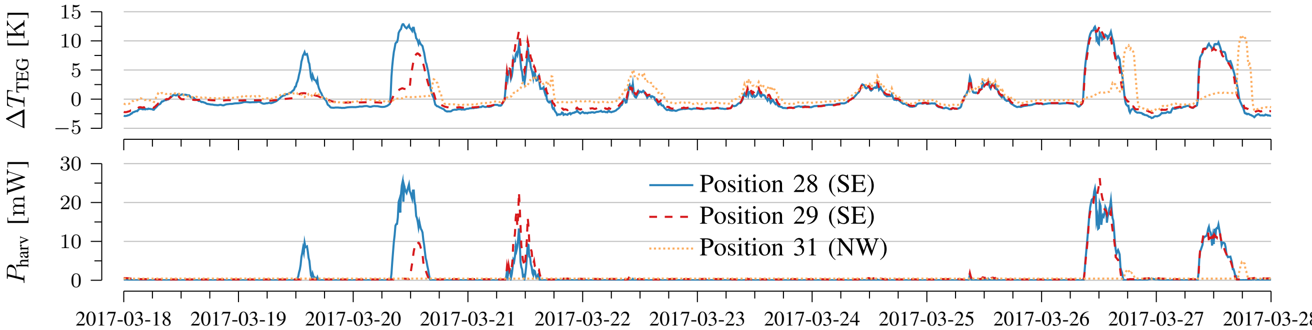

Figure 10. Ten days of temperature difference and resulting harvested power showing the influence of weather and location.

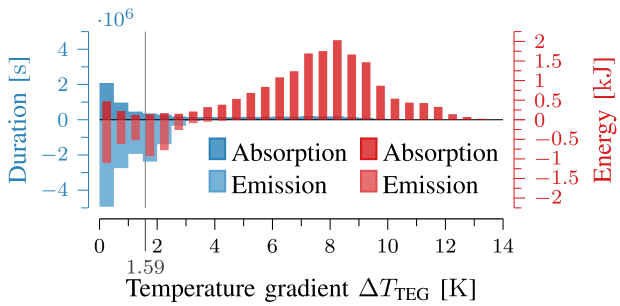

Figure 11. Histogram of temperature gradients and generated energy during 237 days, SE facing sensor node deployment.

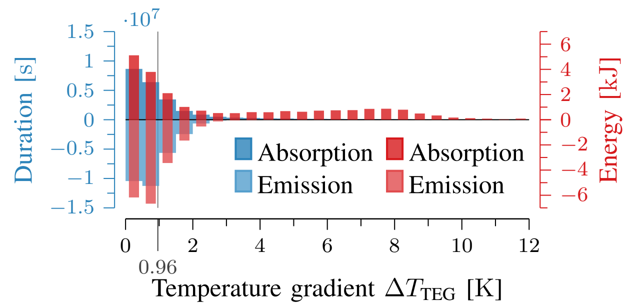

Figure 12. Histogram of temperature gradients and generated energy during 625 days, NW facing sensor node deployment.

in net absorption, harvesting on average $0.96\,\text{mW}$. The SE facing node harvests on average $2.71\,\text{mW}$ in net absorption that occurs during $32.4\,\%$ of the experiment duration, and on average $0.32\,\text{mW}$ in net emission. The shorter time in net absorption and smaller harvested power in net emission are a result of the experiment duration that was dominated by winter where snow cover insulated the radiator.

Comparison Due to the numerous design parameters like material, geometry, or thermal contact, to name a few, a detailed comparison is scope of future work. Nevertheless, a comparison with other TEG based systems of a comparable form factor provides a relation to previous work. With an average harvesting power of $1.1\,\text{mW}$ the presented system significantly outperforms the system described in [23]. Their system was slightly larger and generated on average $0.575\,\text{mW}$. Although the average power is identical to what was achieved in [18], their system had a larger radiator area. Similarly, the experimentally observed peak harvesting power of $27.2\,\text{mW}$ presents the highest value reported in literature for thermoelectric energy harvesting at the ground-to-air boundary with systems that are of comparable size. A systematic comparison to different harvesting modalities, e.g. photovoltaic cells, is highly challenging as numerous factors have to be considered simultaneously. Comparison by area does not suffice, as further aspects including spectral properties, converter architectures, illumination or temperature impact the harvesting efficiency. Developing an appropriate metric and method that incorporates the necessary factors, enables a detailed comparison between different types of harvesting modalities.

VI. Conclusion

We introduced an efficient harvesting platform for extracting electrical energy from small bipolar thermal gradients occurring at the ground-to-air boundary. The harvesting architecture was modeled end-to-end from ambient conditions including meteorological data to the wireless sensor node application. Furthermore, a novel low-power circuit was designed for rectifying the small bipolar voltages generated by thermoelectric generators and incorporated in the overall system model. The model was extensively validated both component-wise in a controlled lab environment, as well as overall in a concrete wall scenario. To evaluate real-world performance, the system was dimensioned and implemented for the use-case of an environment monitoring application. In a long-term case study the harvesting systems was deployed with an wireless monitoring application that senses environmental quantities, participates in a multi-hop network and communicates the acquired information. This experimental evaluation demonstrates self-sustainable operation of the monitoring application with a $550\,\mu\text{W}$ energy footprint. Specifically, the platform harvests up to $27.2\,\text{mW}$ in direct sunlight and $6.3\,\text{mW}$ during nighttime, considerably outperforming current state-of-the-art both in terms of average and maximum harvested power.

Acknowledgment

The authors thank Martin Lüthi for insights into thermal modeling, Moritz Thielen for assistance with TEG simulations, Dominik Böhi for his preliminary work, Tonio Gsell for helping with PermaSense questions, Mark Schmid of Befair for granting access to the construction site, SAFT and Texas

Instruments for technical consulting, as well as Alessandro Cicoira and the custodians of HFSJG and Jungfraubahnen for help with the field work.

References

[1] N. A. Bhatti, M. H. Alizai, A. A. Syed, and L. Mottola, "Energy harvesting and wireless transfer in sensor network applications: Concepts and experiences," *ACM Transactions on Sensor Networks*, vol. 12, DOI 10.1145/2915918, no. 3, pp. 24:1–24:40, 2016.

[2] S. Dalola *et al.*, "Autonomous sensor system with power harvesting for telemetric temperature measurements of pipes," *IEEE Transactions on Instrumentation and Measurement*, vol. 58, DOI 10.1109/TIM.2009.2012946, no. 5, pp. 1471–1478, 2009.

[3] W. Wang *et al.*, "Thermoelectric energy harvesting for building energy management wireless sensor networks," *International Journal of Distributed Sensor Networks*, vol. 9, DOI 10.1155/2013/232438, no. 6, p. 232438, 2013.

[4] Y. K. Tan and S. K. Panda, "Energy harvesting from hybrid indoor ambient light and thermal energy sources for enhanced performance of wireless sensor nodes," *IEEE Trans. Ind. Electron.*, vol. 58, DOI 10.1109/TIE.2010.2102321, no. 9, pp. 4424–4435, 2011.

[5] M. Magno *et al.*, "SmarTEG: An Autonomous Wireless Sensor Node for High Accuracy Accelerometer-Based Monitoring," *Sensors*, vol. 19, DOI 10.3390/s19122747, no. 12, p. 2747, 2019.

[6] D. Rowe, "Applications of nuclear-powered thermoelectric generators in space," *Applied Energy*, vol. 40, DOI 10.1016/0306-2619(91)90020-X, no. 4, pp. 241–271, 1991.

[7] D. Rowe, Ed., *Thermoelectrics Handbook: Macro to Nano*. CRC Press, 2005.

[8] M. Thielen *et al.*, "Human body heat for powering wearable devices: From thermal energy to application," *Energy Conversion and Management*, vol. 131, DOI 10.1016/j.enconman.2016.11.005, pp. 44–54, 2017.

[9] F. Deng *et al.*, "Wearable thermoelectric power generators combined with flexible supercapacitor for low-power human diagnosis devices," *IEEE Trans. Ind. Electron.*, vol. 64, DOI 10.1109/TIE.2016.2613063, no. 2, pp. 1477–1485, 2017.

[10] V. Leonov, "Energy harvesting for self-powered wearable devices," in *Wearable Monitoring Systems*, pp. 27–49, Boston, MA, 2011.

[11] A. Hasler, S. Gruber, and W. Haeberli, "Temperature variability and offset in steep alpine rock and ice faces," *The Cryosphere*, vol. 5, DOI 10.5194/tc-5-977-2011, no. 4, pp. 977–988, 2011.

[12] M. A. Green *et al.*, "Solar cell efficiency tables (version 54)," *Prog Photovolt Res Appl*, vol. 27, DOI 10.1002/pip.3171, no. 7, pp. 565–575, 2019.

[13] J. Yan, X. Liao, D. Yan, and Y. Chen, "Review of micro thermoelectric generator," *J. Microelectromech. Syst.*, vol. 27, DOI 10.1109/JMEMS.2017.2782748, no. 1, pp. 1–18, 2018.

[14] G. J. Snyder, "Thermoelectric energy harvesting," in *Energy Harvesting Technologies*, pp. 325–336, Boston, MA, 2009.

[15] B. Buchli, F. Sutton, J. Beutel, and L. Thiele, "Dynamic power management for long-term energy neutral operation of solar energy harvesting systems," in *Proc. 12th ACM Conf. on Embedded Network Sensor Systems - SenSys '14*, DOI 10.1145/2668332.2668333, pp. 31–45, 2014.

[16] P. D. Mikityuk, "Thermoelectric conversion of thermal flows in soil," *Journal of Thermoelectricity*, vol. 1, no. 1, pp. 84–89, 2003.

[17] L. I. Anatychuk and P. D. Mikityuk, "Thermal generators using heat flows in soils," in *Thermoelectrics, 2003 Twenty-Second Int. Conf. on-ICT*, DOI 10.1109/ICT.2003.1287584, pp. 598–601, 2003.

[18] S. A. Whalen and R. C. Dykhuizen, "Thermoelectric energy harvesting from diurnal heat flow in the upper soil layer," *Energy Conversion and Management*, vol. 64, DOI 10.1016/j.enconman.2012.06.015, pp. 397–402, 2012.

[19] S. Pullwitt, U. Kulau, R. Hartung, and L. C. Wolf, "A feasibility study on energy harvesting from soil temperature differences," in *Proc. 7th Int. Workshop on Real-World Embedded Wireless Systems and Networks - RealWSN'18*, DOI 10.1145/3277883.3277886, pp. 1–6, 2018.

[20] J. W. Stevens, "Optimal placement depth for air-ground heat transfer systems," *Applied thermal engineering*, vol. 24, DOI 10.1016/j.applthermaleng.2003.09.004, no. 2, pp. 149–157, 2004.

[21] ——, "Performance factors for ground-air thermoelectric power generators," *Energy Conversion and Management*, vol. 68, DOI 10.1016/j.enconman.2012.12.029, pp. 114–123, 2013.

[22] M. Gao *et al.*, "Harvesting thermoelectric energy from railway track," *Energy*, vol. 180, DOI 10.1016/j.energy.2019.05.087, pp. 315–329, 2019.

[23] Y. Meydbray, R. Singh, and A. Shakouri, "Thermoelectric module construction for low temperature gradient power generation," in *Proc. Int. Conf. on Thermoelectrics*, DOI 10.1109/ICT.2005.1519958, pp. 348–351, Clemson, SC, USA, 2005.

[24] E. Lawrence and G. Snyder, "A study of heat sink performance in air and soil for use in a thermoelectric energy harvesting device," in *Twenty-First Int. Conf. on Thermoelectrics, 2002. Proceedings ICT '02.*, DOI 10.1109/ICT.2002.1190357, pp. 446–449, Long Beach, CA, USA, 2002.

[25] R. Lorenz, "Subsurface ambient thermoelectric power for moles and penetrators," in *2003 IEEE Aerospace Conference Proceedings*, vol. 2, DOI 10.1109/AERO.2003.1235473, pp. 2_637–2_642, Big Sky, Montana, USA, 2003.

[26] A. Moser *et al.*, "Thermoelectric energy harvesting from transient ambient temperature gradients," *Journal of Electronic Materials*, vol. 41, DOI 10.1007/s11664-011-1894-4, no. 6, pp. 1653–1661, 2012.

[27] U. Datta, S. Dessouky, and A. T. Papagiannakis, "Thermal energy harvesting from asphalt roadway pavement," in *Advancement in the Design and Performance of Sustainable Asphalt Pavements*, pp. 272–286, Cham, 2018.

[28] J. Kim, S.-T. Lee, S. Yang, and J. Lee, "Implementation of thermal-energy-harvesting technology on pavement," *Journal of Testing and Evaluation*, vol. 45, DOI 10.1520/JTE20140396, no. 2, 2016.

[29] M. E. Kiziroglou *et al.*, "Design and fabrication of heat storage thermoelectric harvesting devices," *IEEE Trans. Ind. Electron.*, vol. 61, DOI 10.1109/TIE.2013.2257140, no. 1, pp. 302–309, 2014.

[30] L. V. Allmen *et al.*, "Aircraft strain WSN powered by heat storage harvesting," *IEEE Trans. Ind. Electron.*, vol. 64, DOI 10.1109/TIE.2017.2652375, no. 9, pp. 7284–7292, 2017.

[31] G. Verma and V. Sharma, "A novel thermoelectric energy harvester for wireless sensor network application," *IEEE Trans. Ind. Electron.*, DOI 10.1109/TIE.2018.2863190, pp. 1–1, 2018.

[32] P. Martin, Z. Charbiwala, and M. Srivastava, "DoubleDip: Leveraging thermoelectric harvesting for low power monitoring of sporadic water use," in *Proc. 10th ACM Conference on Embedded Network Sensor Systems*, DOI 10.1145/2426656.2426679, pp. 225–238, 2012.

[33] D. Salerno, "Ultralow voltage energy harvester uses thermoelectric generator for battery-free wireless sensors," *LT Journal of Analog Innovation*, vol. 20, no. 3, p. 1, 2010.

[34] P. Horowitz and W. Hill, *The Art of Electronics*, 3rd ed. New York, NY, USA: Cambridge University Press, 2015.

[35] T. T. Toh *et al.*, "A dual polarity, cold-starting interface circuit for heat storage energy harvesters," *Sensors and Actuators A: Physical*, vol. 211, DOI 10.1016/j.sna.2014.02.037, pp. 38–44, 2014.

[36] C. Peters, J. Handwerker, D. Maurath, and Y. Manoli, "A sub-500 mv highly efficient active rectifier for energy harvesting applications," *IEEE Transactions on Circuits and Systems I: Regular Papers*, vol. 58, DOI 10.1109/TCSI.2011.2157739, no. 7, pp. 1542–1550, 2011.

[37] S. S. Hashemi, M. Sawan, and Y. Savaria, "A high-efficiency low-voltage cmos rectifier for harvesting energy in implantable devices," *IEEE Transactions on Biomedical Circuits and Systems*, vol. 6, DOI 10.1109/TBCAS.2011.2177267, no. 4, pp. 326–335, 2012.

[38] M. Lossec, B. Multon, H. Ben Ahmed, and C. Goupil, "Thermoelectric generator placed on the human body: System modeling and energy conversion improvements," *The European Physical Journal Applied Physics*, vol. 52, DOI 10.1051/epjap/2010121, no. 1, p. 11103, 2010.

[39] S. Gruber *et al.*, "Surface temperatures in steep alpine rock faces - a strategy for regional-scale measurement and modelling," *Proc. 8th Int. Conf. on Permafrost*, vol. 1, pp. 325–330, 2003.

[40] W. Brutsaert, "On a derivable formula for long-wave radiation from clear skies," *Water Resources Research*, vol. 11, DOI 10.1029/WR011i005p00742, no. 5, pp. 742–744, 1975.

[41] M. Sugita and W. Brutsaert, "Cloud effect in the estimation of instantaneous downward longwave radiation," *Water Resources Research*, vol. 29, DOI 10.1029/92WR02352, no. 3, pp. 599–605, 1993.

[42] W. Gray and R. Müller, "Direct radiative transfer," in *Engineering Calculations in Radiative Heat Transfer*, pp. 26–45, 1974.

[43] Texas Insturments, "Bq25570: Nano power boost charger and buck converter for energy harvester powered applications," 2013. [Online]. Available: https://www.ti.com/lit/ds/symlink/bq25570.pdf

[44] J. Beutel *et al.*, "PermaDAQ: A scientific instrument for precision sensing and data recovery in environmental extremes," in *Proc. 2009 Int. Conf. on Information Processing in Sensor Networks*, pp. 265–276, 2009.